The effects of Ti addition and high Cu/Sn ratio on tube type $(Nb,Ta)_3Sn$ strands, and a new type of strand designed to reduce unreacted Nb ratio

Xingchen Xu, Edward Collings, Michael Sumption, Chris Kovacs and Xuan Peng

***Abstract*—In this work we report the properties of two tube type Ta doped Nb_3Sn strands: one strand was additionally Ti doped by way of a Sn-Ti alloy core, and the other had high Cu/Sn ratio within the filaments. Higher irreversibility field (B_{irr}) was obtained on the quaternary strand with respect to the (Nb-7.5wt.%Ta)$_3$Sn strand. High Cu/Sn ratio decreased the amount of coarse grain (CG) formation, but also degraded the layer J_c of the tube type strand by depressing the Sn content in the fine grain (FG) layer. A new type of strand, the subelement of which is composed of 7 bare Cu-Sn cored Nb tube filaments, was designed with the aim to reduce the unreacted Nb area fractions. The test results of the first experimental strand are reported. The unreacted Nb ratio is reduced relative to normal tube type strands and the FG area fraction is improved. The unique structure of this strand makes it also possible to improve the stoichiometry of FG and reduce the effective diameter (d_{eff}).**

***Index Terms*— irreversibility field; layer J_c; Nb_3Sn; tube type.**

I. INTRODUCTION

ALTHOUGH the rod-in-tube (RIT) or restack-rod-process (RRP) Nb_3Sn strands generally have large effective subelement diameters (d_{eff}) and thus poor low field stability [1]-[3], they are the principle Nb_3Sn strands presently being considered for the high energy physics (HEP) applications thanks to their high critical current density J_c [4], [5]. On the other hand, although the non-Cu J_cs of the best powder-in-tube (PIT) and tube type strands are somewhat lower than the best RIT strands, their fine grain (FG) layer J_cs are comparable [6], [7]. In work [6] we show that both the stoichiometry and the grain sizes of the best RIT and tube type strands are similar. This offers the possibility of improving the non-Cu J_c of tubular strands by suitable adjustment of the architecture of the subelements. There are two reasons for the lower FG area fractions in tubular strands: the relatively high unreacted Nb and coarse grain (CG) area fractions.

In work [8] a model predicting the amounts and radial extents of CG and FG areas as functions of the starting Cu and Sn amounts in the filament is presented, and it contends that elevated Cu/Sn ratios diminish the formation of CG and increase the FG area fractions. In this work a strand with high Cu/Sn ratio was tested to find out whether the high layer J_c can be maintained as the Cu/Sn ratio is increased.

We also analyze the reason why tubular strands have higher unreacted Nb area fractions than RIT strands, and then offer a new type of strand that not only reduces the unreacted Nb ratio with respect to normal tube type strands but also decreases the persistent-current magnetization with respect to RIT strands.

The effects of Ti doping on tube type strands are investigated. In a (Nb-7.5 wt.%Ta)$_3$Sn RIT strand improved irreversibility field (B_{irr}) was reported due to Ti addition from the inclusion of Nb-Ti filaments in the starting billet [9]. In this work Ti was introduced into the tube type strands by way of a Sn-Ti alloy core. The effects of Ti doping on B_{irr} and J_c of $(Nb,Ta)_3Sn$ tube type strands are reported.

II. STRAND SPECIFICATIONS AND EXPERIMENT DETAILS

A. Strands prior to heat treatment

Four strands were studied in this work, with their specifications presented in Table I. All of them are Ta doped by using Nb-7.5 wt.% Ta filaments. T1505 is a standard tube type strand with the highest 12 T non-Cu J_c and serves as the benchmark in this work. T2631 is additionally Ti doped via using Sn-1.5 at.% Ti alloy in the core. The strand T2637 has a very high Cu/Sn ratio within the filaments. In addition, a new type T3203 strand, the subelement of which is composed of seven very high Sn/Nb ratio tube type filaments (without Cu matrix), was also studied. The SEM images of subelements (or filaments) of these strands prior to the heat treatments are shown in Fig. 1.

TABLE I HERE
FIG. 1 HERE

B. Heat treatments and measurements

All these strands were wound and heat treated on ITER barrels [10]. Except T3203, which was reacted at 650 °C for 120 h, other strands were all reacted at 625 °C. The reaction times for T1505, T2631, and T2637 were 500 h, 150 h, and 150 h, respectively. Detailed descriptions of preparations, transport measurements and SEM observations can be found

Manuscript received July 16th, 2013. This work was supported in part by the U.S. Dept. of Energy, Office of High Energy Physics, under Grants No. DE-FG02-95ER40900 (OSU) and a DOE SBIR.

X. Xu, E. Collings, M. Sumption and C. Kovacs are with the Ohio State University, Columbus, Ohio 43202 USA (X. Xu phone: 515-441-3429; e-mail: xu.452@osu.edu).

X. Peng is with Hyper Tech Research Inc., Columbus, Ohio, USA.

in [6]. In the energy dispersive spectroscopy (EDS) analysis, to minimize the interaction volume the accelerating voltage of 15 kV was used, leading to an interaction radius of ~0.6 μm according to the Monte-Carlo simulation.

III. RESULTS AND DISCUSSION

The SEM images of these strands after heat treatments are shown in Fig. 2 (a)-(d). The non-Cu $J_c(B)$ curves at 4.2 K of these strands are shown in Fig. 3. The Sn contents in Cu-Sn cores, A15 fine grain sizes, and subelement components fractions of these strands are summarized in Table II, along with the transport measurement results. In a fully reacted tube type strand, the Sn content in the remaining Cu-Sn core is below 2 at.% [8]. From the Sn contents in Cu-Sn cores shown in Table II we see that both T2631-625x150 h and T2637-625x150 h were under-reacted. To make a fair comparison among these strands, the 12 T layer J_cs of these strands were calculated and also shown in Table II. The B_{irr}s (after self-field correction) were obtained by extrapolating the Kramer plots to zero, the validity of which is proved by the linearity of Kramer plots. For tube type strands in which both FG and CG are present, to avoid an overestimation of the FG layer J_c, the CG is assumed to carry 10% of the current density of FG, as explained in detail elsewhere [6].

FIG. 2 HERE
TABLE II HERE
FIG. 3 HERE

A. *The effects of Ti doping*

Fig. 4 presents the Kramer plots of T2631-625x150 h and T1505-625x500 h (both were calculated using FG layer J_cs). It is clear that the low field (<14 T) FG layer J_c of T2631-625x150 h is below that of T1505-625x500 h. This could be the result of Ti induced increase in grain size. However, it should also be noted that layer J_c could be improved with reaction time while the FG layer is still growing [11]. We estimate that the FG layer growth of T2631-625x150 h was nearly 90% complete and further reaction may lead to a several percent improvement in layer J_c. On the other hand, the slope of the Kramer plot of T2631-625x150 h is smaller, leading to a higher extrapolated B_{irr}, proving that Ti and Ta co-doping could be used to improve the B_{irr} of Nb_3Sn strands.

FIG. 4 HERE

B. *The effects of higher Cu/Sn ratio in subelements*

First, as the starting Cu/Sn ratio (shown in Table I) increases from T1505 to T2637, we see clearly from Table II that the CG area fraction is reduced (note that although T2637 was under-reacted, the formation of CG was complete). This is consistent with the prediction by [8]. On the other hand, the transport results show that the layer J_c, B_{irr} and layer $F_{p,max}$ of T2637-625x150 h are all much smaller than those of T1505-625x500 h. The FG formation in T2637-625x150h has been finished for nearly 80%, and further prolonging the reaction time would lead to less than 10% increase in B_{irr}, so the high Cu/Sn ratio should be the main cause of the low B_{irr}. The EDS data shown in Fig. 5 prove that T2637-625x150 h has a prominent Sn content gradient in FG layer, whereas the gradient is smaller in T2631-625x150 h and is inconspicuous in T1505-625x500 h. A possible reason why elevated Cu/Sn ratio leads to larger Sn content gradient in the FG layer could be this: the activity of Sn in solid Cu-Sn alloy (which is the main Sn source for FG growth after Nb_6Sn_5 completely transforms) is smaller than that in Nb_6Sn_5, resulting in a slower rate to supply Sn for Nb-Sn reaction in the A15/Nb reaction frontier. This would lead to a lower Sn concentration in the produced FG layer. The slower reaction rate in T2637 compared to T1505 was affirmed in this study (not shown in this work). On the other hand, since the grain size of T2637-625x150 h is essentially the same with T1505-625x500 h, we infer that the low layer $F_{p,max}$ of T2637-625x150 h could be due to two reasons: first, the low upper critical field B_{c2} of T2637-625x150 h leads to its low layer $F_{p,max}$ since $F_{p,max}$ is proportional to $B_{c2}^{2.5}$ [12]; second, the fine grains of T2637-625x150 h have larger aspect ratio (~1.85) than T1505-625x500 h (~1.6) as a result of the larger Sn concentration gradient, and the low angle grain boundaries of these columnar grains are less efficient pins [13].

However, it should be noted that the T2637-625x150 h investigated in this study was under-reacted, so further study is needed to find out what ultimate B_{irr} and pinning capacities can be achieved by extending the reaction time. Furthermore, it is also interesting to study whether the Sn content gradient can be suppressed in smaller filaments, in which diffusion distance is shorter.

FIG. 5 HERE

C. *A new type of strand*

One cause for the high unreacted Nb area fractions in tubular (PIT and tube type) strands is the shape dissimilarity between the A15 and the Nb tube. In these strands the round front of the growing Nb_3Sn layer touches the edges of the hexagonal Nb area before the Nb in the corners can transform into Nb_3Sn. In contrast, RIT strands have more or less hexagonal A15 layers, leading to an unreacted Nb layer of almost uniform thickness for protection against Sn leakage.

One cure for the dissimilarity problem in tubular strands is the use of round filaments instead of hexagonal ones. Another is to design the subelement structure in this work to enable the formation of hexagonal A15 layers. In this type of strand, each subelement is composed of seven bare Cu-Sn cored Nb tube filaments, as shown in Fig. 6. During the drawing process the starting rods materials (Cu+Sn cores and Nb) flow into and eventually fill all the space. This would cause the Cu+Sn cores of the six outer filaments to become “dumpling-shaped”, as shown in Fig. 1 (d). Then during heat treatment, the A15 areas of the six outer filaments eventually turn into flat frontiers, as shown in Fig. 2 (d), forming an almost hexagonal A15/Nb boundary, just like the RIT strands.

FIG. 6 HERE

The first experimental strand we produced along these lines, T3203, was reacted for 120 h at 650 °C, leading to a non-Cu J_c of 2350 A/mm^2 at 4.2 K, 12 T. Further improvement is expected by improving the fabrication quality. From Table II we see that the unreacted Nb fraction is reduced to 14%, and the FG area fraction is raised to 46%. At this point we need to correct a misleading statement we made in [6]. The FG area fraction of a tubular strand cannot be enlarged to 60% (the typical level in RIT strands) by simply reducing the unreacted Nb area fraction. This is because the core, CG, and FG area fractions increase together as the unreacted Nb area decreases. For instance, our calculation shows that for a tube type strand with a typical Cu/Sn ratio, the FG area fraction can only be improved to 50% as the unreacted Nb is reduced to 8 % (the typical level of RIT strands). Further improvement in FG area fraction needs reduction of the CG area by raising the Cu/Sn ratio [8].

Returning to T3203 we note in Fig. 3 that the $J_c(B)$ curve of T3203-650x120 h has a smaller slope than the other strands. Although the lack of data below 9 T prevents the construction of a Kramer plot, it is clear that its B_{irr} is even higher than T2631-625x150 h. The possible reason for the enhanced B_{irr} of T3203 lies in its unique subelement structure such that the local Sn/Nb ratio inside the Nb barrier is very high. During reaction this would lead to improved stoichiometry.

Another potential advantage of this new strand is smaller persistent-current magnetization compared to an RIT strand with the same geometric subelement diameter d_{sub} and J_c. In RIT strands the central hole of a subelement causes the effective diameter d_{eff} to be 10-20% larger than the d_{sub} [3], while in this new type of strand this hole area is broken into seven, with six of them far from the center, which would cause significant decrease in the magnetization.

The strand T3203 has 61 subelements. However, considering HTR has produced tube type strands with 1387 filaments without any problem [14], we expect a successful production of this type of strand with 217 subelements in a 0.7 mm strand diameter.

IV. SUMMARY

Ti addition via Sn-Ti alloy improves the B_{irr} of $(Nb,Ta)_3Sn$ tube type strands and thus benefits high field J_c. Enhancing Cu/Sn ratio within the filaments reduces the formation of CG, but also decreases the Sn content in the FG layer and thus is not beneficial for the layer J_c. A new type of strand was designed. This type of strand has smaller unreacted Nb ratio with respect to the normal tube type strands, and also achieves better stoichiometry and B_{irr} than normal Nb_3Sn strands.

ACKNOWLEDGMENT

The authors thank David Gladysz of Hyper Tech Research Inc. for heat treating these strands.

REFERENCES

[1] A. K. Ghosh, L. D. Cooley, A. R. Moodenbaugh, J. A. Parrell, M. B. Field, Y. Zhang, and S. Hong, "Magnetization studies of high J_c Nb_3Sn strands," *IEEE Trans. Appl. Supercond.*, vol. 15, no. 2, pp. 3494–3497, Jun. 2005.

[2] L. D. Cooley, P. S. Chang, and A. K. Ghosh, "Magnetization, RRR and stability of Nb_3Sn strands with high sub-element number," *IEEE Trans. Appl. Supercond.*, vol. 17, no. 2, pp. 2706–2709, Jun. 2007.

[3] B. Bordini, D. Richter, P. Alknes, A. Ballarino, L. Bottura, and L. Oberli, "Magnetization Measurements of High- J_c Nb_3Sn Strands," *IEEE Trans. Appl. Supercond.*, vol. 23, no. 3, 7100806, Jun. 2007.

[4] S. Hong, M. B. Field, J. A. Parrell, and Y. Zhang, "Latest Improvements of Current Carrying Capability of Niobium Tin and Its Magnet Applications", *IEEE Trans. Appl. Supercond.*, Vol. 16, Issue 2, Pages 1146 – 1151, June 2006.

[5] J. A. Parrell, M. B. Field, Y. Zhang, and S. Hong, "Advances in Nb_3Sn strand for fusion and particle accelerator applications", *IEEE Trans. Appl. Supercond.*, Vol. 15, Issue 2, Part 2, Pages 1200 – 1204, June 2005.

[6] X. Xu, M. D. Sumption, S. Bhartiya, X. Peng, and E. W. Collings, "Critical current densities and microstructures in rod-in-tube and tube type Nb_3Sn strands—present status and prospects for improvement," *Supercond. Sci. Technol.*, Vol. 26, Issue 7, 075015, July 2013.

[7] T. Boutboul, L. Oberli, A. den Ouden, D. Pedrini, B. Seeber, and G. Volpini, "Heat treatment optimization studies on PIT Nb_3Sn strand for the NED project," *IEEE Trans. Appl. Supercond.*, Vol. 19, Issue 3, Pages 2564 – 2567, June 2009.

[8] X. Xu, M. D. Sumption, E. W. Collings, "A Model for Phase Evolution and Volume Expansion in Tube Type Nb_3Sn Conductors," *Supercond. Sci. Technol.*, Vol. 26, Issue 12, 125006, October 2013.

[9] A. K. Ghosh, E. A. Sperry, J. D'Ambra, and L. D. Cooley, "Systematic Changes of the Nb-Sn Reaction With Time, Temperature, and Alloying in Restacked-Rod-Process (RRP) Nb_3Sn Strands," *IEEE Trans. Appl. Supercond.*, Vol. 19, Issue 3, Pages 2580 – 2583, June 2009.

[10] A. Godeke, "Performance Boundaries in Nb_3Sn Superconductors", Ph.D. dissertation, Univ. of Twente, Enschede, The Netherlands, 2005.

[11] C. M. Fischer, "Investigation of the relationships between superconducting properties and Nb_3Sn reaction conditions in Powder-in-Tube Nb_3Sn", Master Thesis, University of Wisconsin-Madison, Madison, Wisconsin, 2002.

[12] W. A. Fietz and W. W. Webb, "Hysteresis in Superconducting Alloys—Temperature and Field Dependence of Dislocation Pinning in Niobium Alloys," *Phys. Rev.*, Vol. 178, Issue 2, Pages 657-667, Feb. 1969.

[13] C. Verwaerde, R. Taillard, C. E. Bmzek, and Hoang-Gia-Ky, "Quantity and quality of the Nb_3Sn intermetallics formed by the internal tin process," *Adv. Cryog. Eng.*, Vol. 42, Pages 1377-1384, May 1997.

[14] X. Peng et al., "Strain and magnetization properties of high subelement count Tube-Type Nb3Sn strands," *IEEE Trans. Appl. Supercond.*, Vol. 21 Issue 3, Pages 2559–2562, June 2011.

TABLE I. SPECIFICATIONS OF THE STRANDS AT FINAL SIZE BEFORE REACTION

Strand	T1505	T2631	T2637	T3203
Strand diameter, mm	0.7	0.7	0.7	0.7
No. of subelements	217	217	217	61
Tin core composition	Pure Sn	Sn-1.5 at.% Ti	Pure Sn	Pure Sn
Filament composition	Nb-7.5 wt.% Ta	Nb-7.5 wt.% Ta	Nb-7.5 wt.% Ta	Nb-7.5 wt.% Ta
Barrier material	-	-	-	Pure Nb
Nb:Sn atomic ratio	4.94:1	5.20:1	5.27:1	3.76:1 [a]
Cu:Sn atomic ratio	0.376:1	0.552:1	1.16:1	0.498:1

[a] Including the Nb barrier.

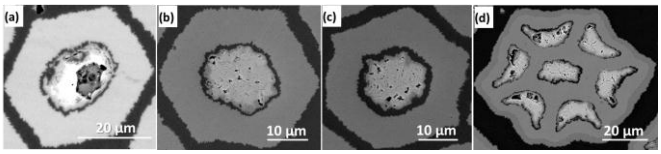

Fig. 1. The SEM images of subelements of (a) T1505, (b) T2631, (c) T2637, and (d) T3203 strands prior to heat treatment.

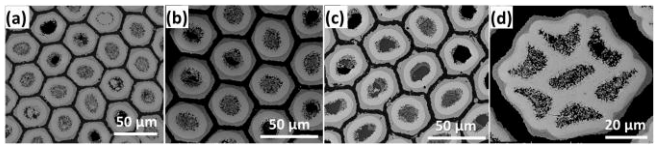

Fig. 2. The SEM images of subelements of (a) T1505-625x500 h, (b) T2631-625x150 h, (c) T2637-625x150 h, and (d) T3203-650x120 h.

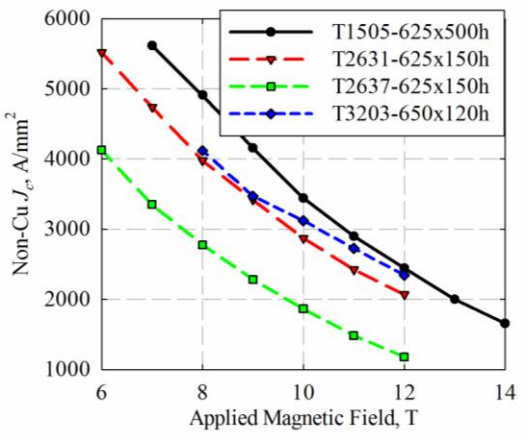

Fig. 3. The non-Cu $J_c(B)$ curves at 4.2 K of T1505-625x500 h, T2631-625x150 h, T2637-625x150 h, and T3203-650x120 h.

TABLE II. THE CU-SN CORECOMPOSITIONS, FG SIZES, AREA FRACTIONS, AND TRANSPORT MEASUREMENT RESULTS OF THESE STRANDS AFTER HEAT TREATMENTS.

Strand	T1505-625x500	T2631-625x150	T2637-625x150	T3203-650x120
Sn content in Cu-Sn core, at.%	2.02	9.85	9.14~21.9 [a]	2.99
Average FG size, nm	103	106	101	119
Unreacted Nb, %	26.1	30.8	37.3	14.0
FG area, %	41.8	36.4	32.0	46.0
CG area [b], %	15.9	13.4	9.6	14.7
Core area [b], %	16.2	19.4	21.1	25.4
4.2 K, 12 T non-Cu J_c, A/mm^2	2440	2070	1180	2350
4.2 K, 12 T layer J_c [c], A/mm^2	5630	5485	3580	4950
Extrapolated B_{irr} [d], T	25.1	26.1	21.8	- [e]
Layer $F_{p,max}$, GN/m^3	97.4	89.6	77.4	- [e]

[a] The Cu-Sn core of T2637-625x150 h is composed of two phases: the bronze (Cu-9.14 at.% Sn) and the γ phase (Cu-21.9 at.% Sn), indicating the transformation from γ phase to bronze is not finished yet.

[b] For tube type strands, the CG area should include both the connected CG region and the disconnected particles dispersed in the Cu-Sn cores. However, here only the fractions of the connected CG regions are given for the convenience of calculating the layer J_cs, cf. [8].

[c] For tube type strands, to avoid an overestimation of the FG layer J_c, the CG area is assumed to carry 10% of the current density of FG area.

[d] The extrapolated B_{irr} values were calculated after self-field corrections.

[e] The extrapolated B_{irr} and layer $F_{p,max}$ values of T3203-650x120 h were not available because the measurements quenched at below 9 T.

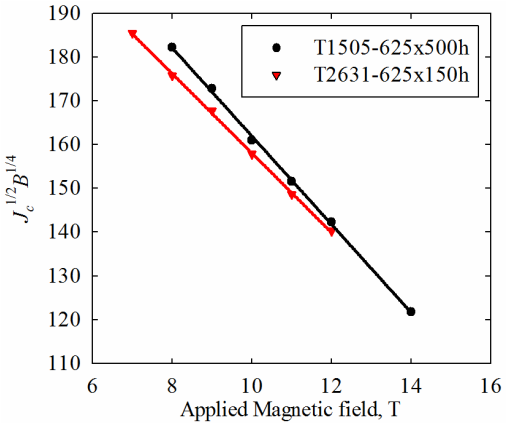

Fig. 4. The Kramer plots of T1505-625x500h and T2631-625x150h at 4.2 K.

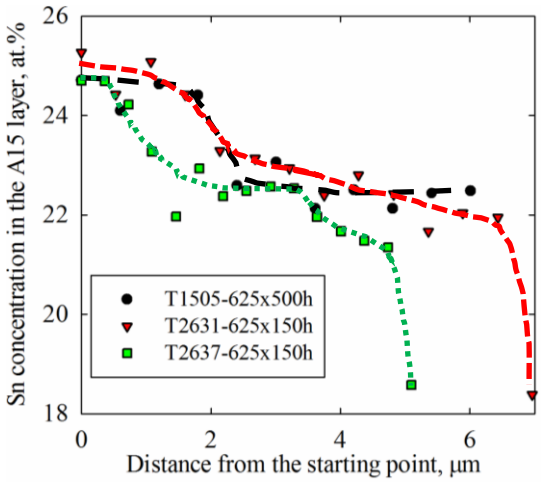

Fig. 5. The Sn concentrations in the A15 layers. Note that the Sn contents are around 25 at.% in CG region, and vary from 18 to 23.5 at.% in the FG regions. The dashed lines serve as guides to the eye.

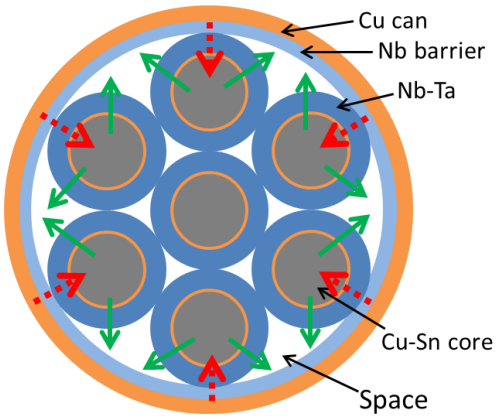

Fig. 6. A schematic of a subelement before drawing process. During the drawing process the six outer filaments are subjected to the compression forces as shown by the red dash arrows, and have materials following in the directions shown by the green solid arrows.